Green Chemistry

PAPER

View Article Online
View Journal | View Issue

Cite this: *Green Chem.*, 2022, **24**, 6189

An experimental and modeling study on the catalytic effects of select metals on the fast pyrolysis of hardwood and softwood lignin†

Sean A. Rollag,‡[a] Keunhong Jeong, ‡[b] Chad A. Peterson,[c] Kwang Ho Kim [d] and Robert C. Brown *[a,c]

Naturally occurring alkali and alkaline earth metals (AAEM) play an important catalytic role in the pyrolysis of lignin. Other metals also potentially play a role in the catalytic deconstruction of lignin but have only been qualitatively investigated. A combination of experiments and computational modeling were performed to explore the catalytic activity of ferrous iron in comparison to AAEM. Pyrolysis experiments with extracted lignin and density functional theory (DFT) calculations for model lignin dimers showed agreement between theory and experiment. Ferrous iron proved to be a stronger catalyst than either potassium or calcium. The activity order of the AAEM cations was less clear as model and experiments agreed for hardwood lignin but disagreed for softwood lignin. DFT predicted calcium to be a stronger catalyst than potassium for breaking β-O-4 ether bonds while experiments indicated potassium to be more catalytically active as a result of higher turnover frequency. Pyrolysis of softwood lignin had a lower apparent activation energy (9.2 kcal mol^{-1}) than for hardwood lignin (15.3 kcal mol^{-1}). Of the catalysts tested only ferrous iron prevented the melting of lignin during pyrolysis due to its low apparent activation energy of 3.6 kcal mol^{-1} and 8.6 kcal mol^{-1} for softwood and hardwood lignin, respectively.

Received 26th December 2021,
Accepted 30th June 2022

DOI: 10.1039/d1gc04837f

rsc.li/greenchem

1 Introduction

Since its identification over 200 years ago,[1] lignin has been the subject of many largely unsuccessful attempts to exploit its unique biochemical properties. Given the difficulties of overcoming its recalcitrant structure, the most common use of lignin is generation of process heat for paper mills and cellulosic ethanol plants. If viable methods for depolymerizing lignin can be developed, lignin would be greatly valorized.[2]

The natural recalcitrance of lignin to biological deconstruction[3] makes thermochemical processing an attractive pathway for deconstruction. Fast pyrolysis, which uses thermal energy and sometimes catalysts to break intermolecular bonds, is among the most attractive thermochemical processes for valorizing lignin. However, the tendency of lignin to melt when heated complicates its thermal depolymerization. Technical lignin as well as biomass from which alkali and alkaline earth metals (AAEM) have been extracted have been widely observed to liquefy and foam during pyrolysis.[4–6] Dehydration reactions carbonize this foamed lignin to form large char agglomerates that can reduce reactor throughput or even plug the reactor.[5] Some mechanical systems are aggressive enough to break apart these agglomerates,[7] but this solution adds complexity, accelerates equipment wear, and does not fully restore reactor throughput.

Pretreatment of lignin is a potential solution to this agglomerating behavior. Empirical research has discovered several effective pretreatments. Physical pretreatments add inert material such as fumed silica[8] or clay[9] to dilute the lignin and increase its surface area as it melts, increasing the rate of vaporization. Alternatively, chemical agents such as calcium hydroxide can catalyze lignin deconstruction reducing the size of agglomerates and partially mitigating the problem.[10] However, more effective approaches to catalytic depolymerization could improve the commercial prospects of lignin pyrolysis.

Few previous studies have modeled the catalytic interaction between metal ions and lignin. Kim *et al.*[11] found that Na and Mg, naturally occurring metals in biomass, were very effective in catalyzing deconstruction of lignin. Later research by Jeong *et al.*[12] modeled the catalytic behavior of AAEM during biomass pyrolysis. They found alkaline metals to be more powerful than alkaline earth metal in catalyzing lignin deconstruction. We have found iron in the form of ferrous salts to be

[a]*Department of Chemical and Biological Engineering, Iowa State University, Ames, IA, USA. E-mail: rcbrown3@iastate.edu*
[b]*Department of Chemistry, Korea Military Academy, Seoul, Republic of Korea*
[c]*Bioeconomy Institute, Iowa State University, Ames, IA, USA*
[d]*Clean Energy Research Center, Korea Institute of Science and Technology, Seoul, Republic of Korea*

†Electronic supplementary information (ESI) available. See DOI: https://doi.org/10.1039/d1gc04837f

‡These authors equally contributed to this work.

an effective alternative to AAEM in the catalytic depolymerization of lignin in whole biomass.[13] However, to be effective, ferrous cations had to be added at much higher molar concentrations than alkali metals.[14] There was also found a correlation between the amount of ferrous cation required and the syringyl lignin content of the biomass.[14] Understanding this catalytic behavior could help unlock new deconstruction paths for lignin.

The goal of this study is to understand the role of ferrous iron in catalyzing rapid lignin depolymerization and preventing char agglomeration during pyrolysis of biomass. Additionally, hardwood and softwood lignins were investigated to understand how catalytic depolymerization is influenced by different kinds of lignin in biomass. Insights from DFT modeling of metal-catalyzed lignin depolymerization are compared to experimental results from micropyrolysis of extracted lignin in the presence of catalysts.

2 Materials and methods

2.1 Density functional theory model

Density functional theory (DFT) calculations were performed on the decomposition of lignin model dimers into monomers. Guaiacylglycerol-β-guaiacyl ether (GGE) and syringylglycerol-β-syringyl ether (SSE) were chosen as representative lignin model dimers. Considering the complex structure of macromolecular lignin, β-O-4 dimeric model compounds were employed for the computational study. Two β-O-4 model dimers (GGE and SSE) are commonly used for the mechanistic study because they account for 50–80% of interunit linkages. Therefore, it is believed that an in-depth analysis of β-O-4 models can provide mechanistic insights into macromolecular lignin. The M06-2X hybrid exchange–correlation functional was used with the LanL2DZ basis set for ferrous ions and the 6-311++G(d, p) basis set for potassium and calcium ions in the Gaussian 16 program.[15] Starting geometries of the lignin–metal complex, in which metal ions bind with O(C_β) and O(methoxyl) of the model dimer, were built based on their previously determined structures.[11] After determining the local energy minima for each structure with no imaginary frequencies, the binding energy and structural information were determined. To calculate Wiberg bond order (WBO) index for each structure, Bader's atoms-in-molecule (AIM) analysis calculation was performed to compare the strength of bonding in the complexes by using the Multiwfn program.[16] Weinhold natural population analyses (NPA) were carried out using the NBO 3.1 module embedded in the Gaussian 16 packet to better comprehend the bonding and electronic properties of the complexes.[17]

2.2 Milled wood lignin extraction

Lignin from red oak (*Quercus rubra*) and loblolly pine (*Pinus taeda*) was extracted using the Bjorkman milled wood lignin (MWL) extraction method.[18] Biomass was ball milled in a Retsch planetary ball mill until a fine powder remained. The milled wood in the amount of 100 g was combined with 1L methanol and mixed for 24 hours with a magnetic stir bar. The solution was then centrifuged, and the methanol decanted. Fresh methanol (1 L) was added to the biomass and the mixture stirred for another 24 h. The recovered solids were dried in a vacuum oven at 40 °C. The dried material was ball milled in alternating 15-minute sessions of milling and resting for a total of 72 h of milling. The material was then dissolved in a 1 L solution of 96% 1,4-dioxane and 4% water and mixed for 24 hours. Solids were recovered *via* vacuum filtration and dispersed in 1 L fresh dioxane, stirred for 24 h, filtered, and the filtrate dried in a rotary evaporator. The resulting crude lignin was dissolved in 100 mL of 90% acetic acid and the solution added dropwise to 1 L cold water which caused the lignin to precipitate. The precipitate was recovered *via* centrifugation and dried again at 40 °C in a vacuum oven. The dry material was mixed with 50 mL of a 2 : 1 solution of 1,2-dichloroethane and ethanol which dissolved the milled wood lignin leaving behind a solid residue that was removed by centrifugation. Adding the supernatant dropwise to 1 L of anhydrous ethyl ether cause precipitation of purified MWL which was recovered by centrifugation and vacuum oven drying at 40 °C.

2.3 Addition of catalyst to the lignin

Catalyst was added to the lignin samples by infusing acetate salt of the desired metal into the lignin. The cations bind to oxygen atoms in the lignin structure, forming various metal–lignin complexes.[19] This method was similar to that used by Rollag *et al.* for whole biomass.[13] MWL in the amount of 250 mg was mixed with an appropriate amount of an acetate salt to give a loading of 1.9 millimoles of catalytic metal atoms per gram of lignin. To this mixture 25 mL of deionized water was added. The mixture was magnetically stirred for 4 h before being poured onto watch glasses and dried in an oven overnight at 105 °C. After drying samples were hand ground back to powder form to ensure particle size did not impact the testing.

2.4 Time-resolved devolatilization of lignin depolymerization products

Real-time evolution of vapor products from fast pyrolysis of the lignin samples was accomplished using a modified PY 2020 Frontier micropyrolyzer in combination with a flame ionization detector (FID) as developed by Peterson *et al.*[20] Rather than admitting biomass samples to the micropyrolyzer in a small metal cup, the small particles of biomass were adhered to a sample hook through weak Coulomb forces. As shown in Fig. 1, the hook was installed above the heated furnace zone of the micropyrolyzer in a steady flow of helium. An experiment was initiated by closing a valve that controlled the flow of helium to the micropyrolyzer. After three seconds, the valve was quickly opened, which sent a pulse of gas through the apparatus that dislodged the particles from the hook. The particles were swept downward into the heated zone where they were captured on an array of screens consisting of a copper screen (250 μm mesh) between two stainless-steel screens (90 μm mesh). Given the large mass of the screens (approxi-

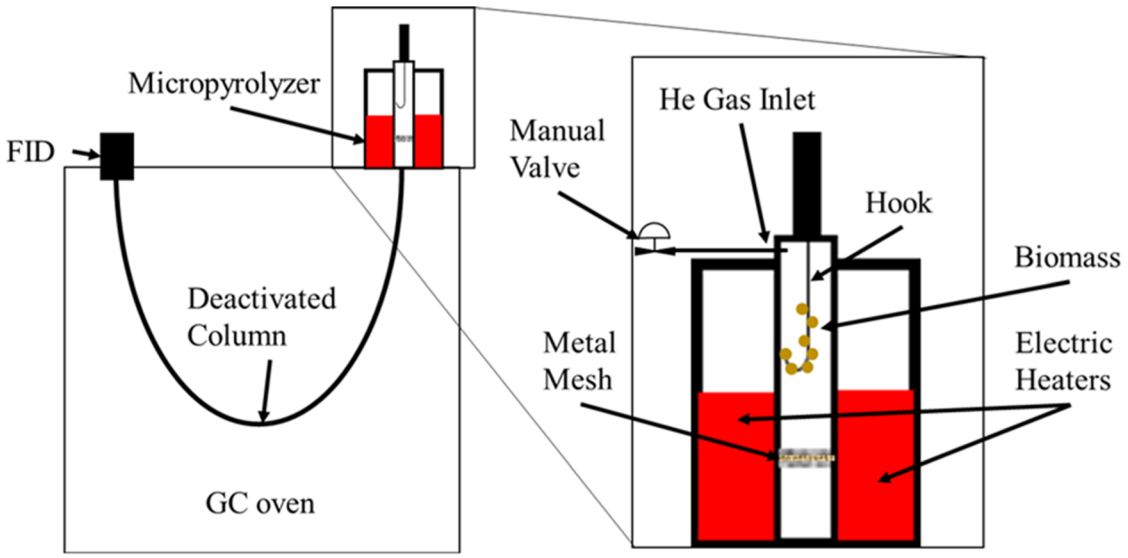

Fig. 1 Diagram of short column GC with modified micropyrolyzer system attached.

mately 100 mg) compared to the sample (approximately 1 mg) the reaction was assumed to be isothermal. The particles rapidly heated and released volatiles that were transported through a deactivated short column (SC) of approximately 0.5 m length housed in a Bruker 430 GC to a FID. The deactivated SC did not separate the volatile products but simply transported them with minimal lag time to the FID, which measured voltage response at 80 Hz resolution. We have previously demonstrated that this "short column micropyrolyzer/FID" apparatus allows time resolved quantification of devolatilization during fast pyrolysis of biomass making possible measurement of pyrolysis reaction rates.[21] Here we use it to determine the effect of metal catalysts on rates of lignin depolymerization into volatile phenolic monomers. Experiments were conducted at 33 °C intervals from 366–500 °C.

The time-resolved FID signal, $S(t)$, is characterized by a rapid rise followed by a more gradual decay. The rise is associated with the lag time of the overall instrumentation while the decay correlates to the progression of sample depolymerization and the devolatilization of the resulting products as long as the reaction time is much longer than the instrument lag time, which we have confirmed in a previous study.[22]

The start of reaction was taken as the time that the FID voltage reached 1% of the maximum recorded signal (representing the maximum measured devolatilization rate). The end of reaction was taken as the time when the FID voltage fell to less than 3% of the maximum reading. The FID signal was normalized based on the maximum signal and used to calculate the extent of reaction:

$$\alpha(t) = \frac{\theta(t)}{\theta_T} \quad (1)$$

where $\theta(t)$ is the integrated FID signal up to time t and θ_T is the integrated FID signal over the total time for reaction. The extent of reaction was numerically differentiated to obtain the corresponding rate of change of the extent of reaction, $d\alpha/dt$. Assuming devolatilization is a first order reaction:

$$\frac{d\alpha}{dt} = k(1-\alpha) \quad (2)$$

where k is the reaction rate coefficient with units of inverse seconds. A non-linear solver (Python 3: SciPy[23]) was used to determine the reaction rate coefficient from the experimental data.

2.5 Truncated pyrolysis

Truncated pyrolysis experiments to investigate structural changes during pyrolysis were performed using the Controlled Pyrolysis Duration-Quench (CPD)-described by Lindstrom *et al.*[21] The system used a computer controlled arm to lower samples in the furnace zone of a Frontier 3030D micropyrolyzer for a prescribed period of time followed by rapid ejection of the sample from the bottom of the furnace to a glass vessel chilled by an ice bath. To ease removal of melted samples for analysis, aluminum foil liners were used inside the standard stainless-steel cups. Lignin samples were ejected from the furnace after 3 s at which point the samples are estimated to have reached 400 °C.[22] At this timescale, the sample had only partially pyrolyzed, with unreacted biopolymers still present in the samples. Other samples were allowed to dwell in the furnace for 60 s, which allowed the samples to reach 500 °C and completely pyrolyze, leaving only biochar. To determine if melting had occurred during pyrolysis the sample cups were overturned and lightly tapped on a hard surface. A sample was determined to have melted is the char remained adhered to the bottom of the sample cup while unmelted samples would pour out loose char. Additionally when the foil liner was removed and flattened for analysis the presence of melted char was visually verified. Melted samples would appear as a thin

film on the surface of the foil, while unmelted samples retained a three-dimensional structure above the surface of the foil.

2.6 Infrared spectrometry

A Fourier Transform Infrared spectrometer (FTIR) (Nicolet Magna-IR 560 Spectrophotometer) was used to probe chemical bonds within the samples. The method collected 64 scans from wavenumber 3700 cm^{-1} to 600 cm^{-1}. Identification of absorption bands was done manually using infrared spectroscopy tables.

3 Results and discussion

3.1 DFT modeling of catalytic interactions of AAEM and ferrous iron

DFT modeling of lignin dimers, GGE (representing softwood) and SSE (representing hardwood), revealed multiple potential binding sites for catalytic ions. The presence of additional methoxy groups in the SSE dimer allowed for two more potential catalyst binding sites than the GGE dimer. Fig. 2 indicates the potential binding sites for these two different dimers. Of these sites the most catalytically relevant locations are 3 and 5, due to their proximity to the bond in question.[11] Sites 3 and 5 also happen to be the most energetically favored according to Gibbs free energy difference calculations (see Table S1† for all values). The calculated values for these two main sites can be found in Table 1.

It is noteworthy that the SSE contains two bonding sites which strongly promote the catalytic activity (increase the bond length of β-O-4 ether). After analyzing the stable structure of binding sites 3 and 5, we conclude that the half-sandwich structure is formed in the 3 position for both cases (GGE and SSE), additionally, between ferrous iron and oxygen in SSE on binding site 5 (Fig. 3). WBO information for ferrous iron binding with each model molecule indicates that it is forming strong half-sandwich complexes (average WBO is 0.144 for Fe(II)-GGE and 0.146 for Fe(II)-SSE) compared to the small average WBO of 0.06 and 0.083 for K(I) and Ca(II), respectively. These differences in average WBO indices compare with the bonding energies observed for the metal ions binding in position 3. For the position 5, unlike the other binding positions (1, 2, and 4) with two bonds, its complex is composed of 3 intramolecular bonds, which explains the additional stable structure that should be considered for estimating the catalytic effect.

Further theoretical NBO was done to investigate why the 5-position induced longer bond lengths during pyrolysis than position 3. Theoretically calculated charges in each structure shows that the stronger positive charge in ferrous iron induces an increased negative charge in the oxygen of β-O-4 ether bond. These stronger charges ultimately weaken the covalent bond. This result provides important information for obtaining new catalytic effects from various metal ions for future analysis of lignin deconstruction (Fig. 4).

Table 1 DFT calculated values of catalyst binding affinity and the resulting length of the β-O-4 ether bond. Values for bind to site 3 for the GGE model and site 3 and 5 for the SSE model

Dimer	Catalyst	Gibbs free energy difference [kcal mol^{-1}]	Bond length [Å]
GGE	None	NA	1.427
	Ferrous iron [Fe^{2+}] (3)	−301.52	1.479
	Calcium [Ca^{2+}] (3)	−162.62	1.465
	Potassium [K^{+}] (3)	−34.163	1.442
SSE	None	NA	1.425
	Ferrous iron [Fe^{2+}] (3)	−313.96	1.477
	Ferrous iron [Fe^{2+}] (5)	−295.47	1.484
	Calcium [Ca^{2+}] (3)	−173.36	1.462
	Calcium [Ca^{2+}] (5)	−171.84	1.476
	Potassium [K^{+}] (3)	−38.31	1.440
	Potassium [K^{+}] (5)	−37.33	1.447

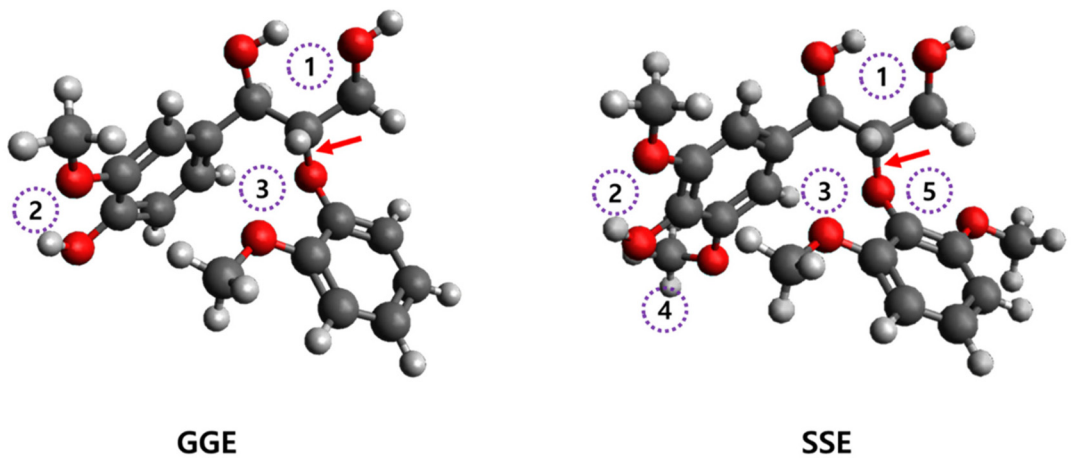

Fig. 2 GGE (Left) and SSE (Right) lignin model dimers with OFT calculated metal catalyst binding sites. The β-O-4 ether bond broken during pyrolysis is denoted by the red arrow in each molecule.

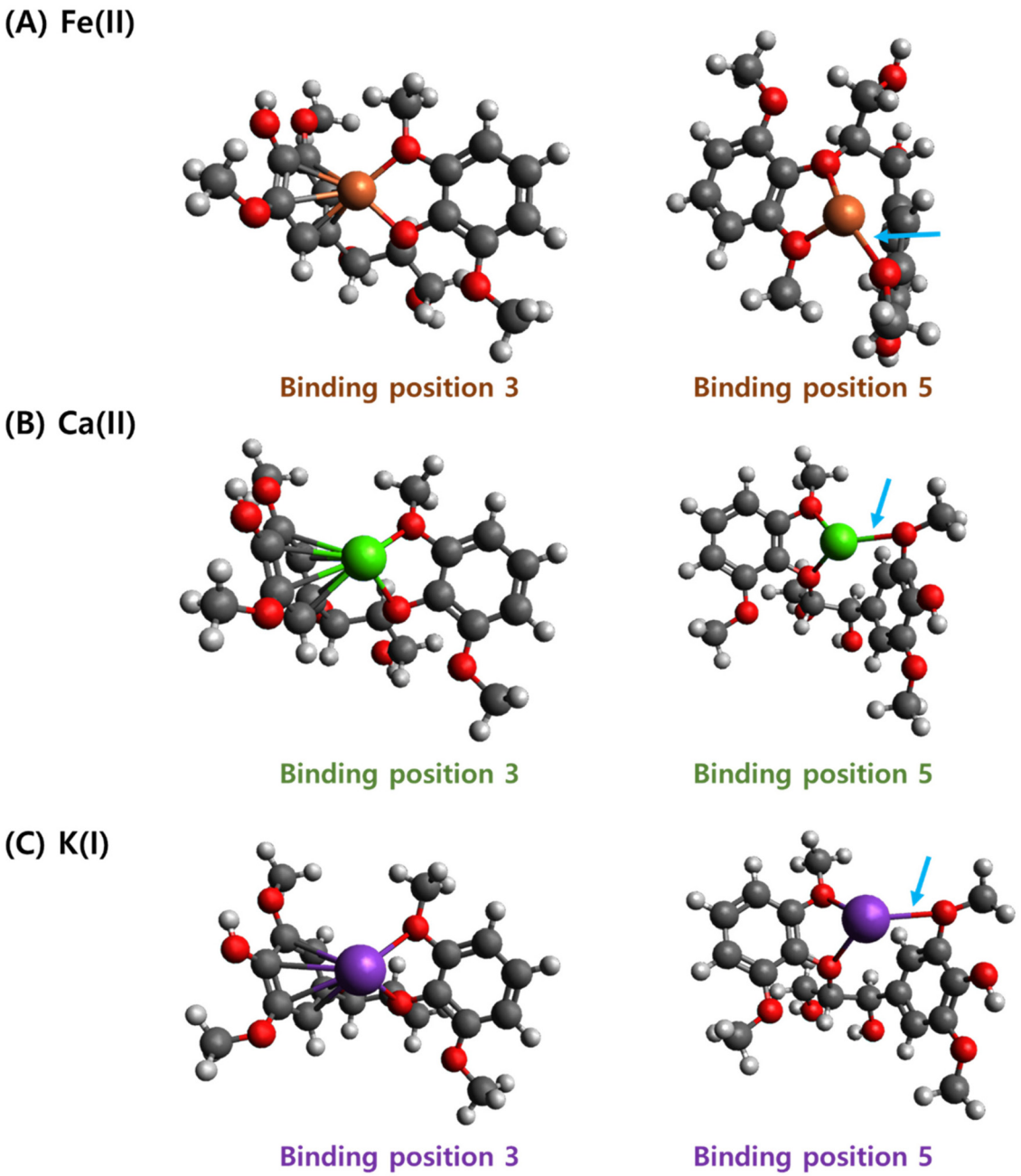

Fig. 3 Optimized each metal-SSE complexes for different binding position with (A) Fe(II), (B) Ca(II), and (C) K(I). It shows the additional half-sandwich structure for position 3 and one more chemical bond (light blue arrow) for position 5.

From the above analysis, ferrous iron was determined to have the greatest affinity for binding to lignin with a Gibbs free energy of around −304 kcal mol^{-1}. Calcium's affinity was only about half that of ferrous iron at approximately −169 kcal mol^{-1}. While potassium only weakly binds to lignin having a Gibbs free energy of only about −37 kcal mol^{-1}. The bond length difference between the softwood model and the hardwood model was minimal at only 0.002 Å. Although relatively minor, this suggests that the ether bonds in softwood lignin are easier to break than hardwood lignin. When metals were bond to the dimer systems there was a significant stretching of the C_β–O bond. This stretching destabilizes the bond by lowering the dissociation energy (activation energy), making it easier to break. Somewhat surprisingly, DFT modeling indicates that ferrous iron is the strongest of the catalysts investigated. For both lignin dimers ferrous iron was the strongest catalyst followed by calcium and potassium, respectively. This finding was contrary our expectation based on previous research[14] that ferrous iron was a weaker catalyst than the native AAEM.

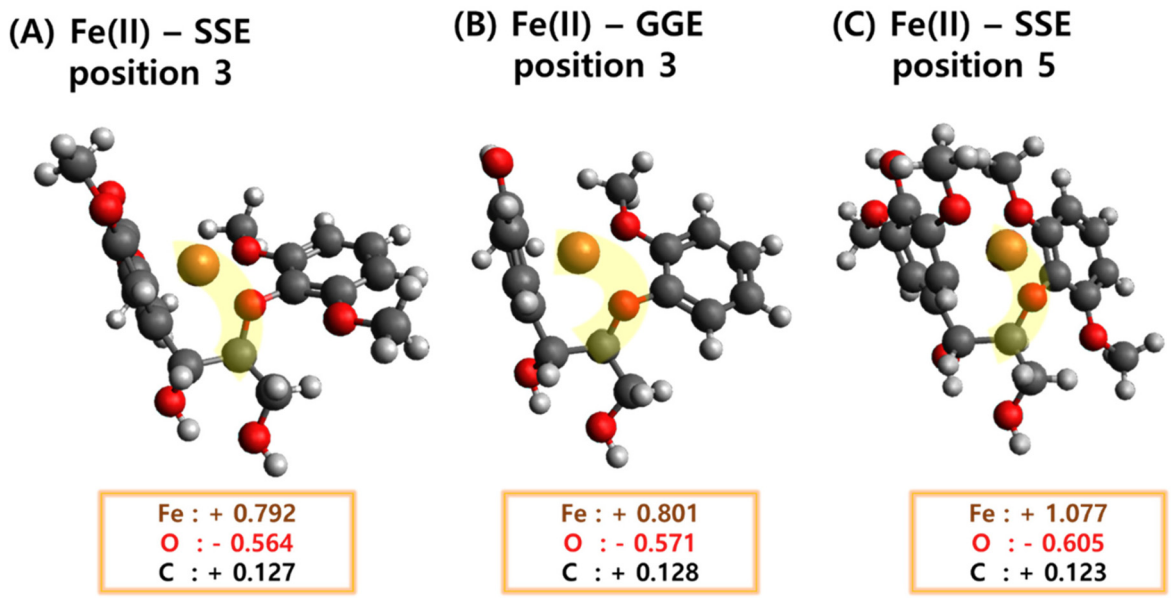

Fig. 4 Optimized structures for Fe(II) with GGE and SSE. Highlighted atoms are ferrous iron, oxygen, and carbon. Atomic changes for each structure support the bond length difference.

One potential reason for this discrepancy might arise from differences in dispersion of the metal ions in real biomass. Naturally incorporated AAEM in whole biomass is likely to be heterogeneously dispersed into various components of the cell wall. While the method used to infuse ferrous iron more homogeneous dispersion of metal ion throughout the biomass. The addition of ferrous iron beyond the molar concentrations typical of naturally occurring AAEM likely results in its nonproductive binding to other components of the biomass such as cellulose. This artifact of the incorporation process would make ferrous iron appear to be less effective than AAEM.

3.2 Apparent activation energies of extracted lignin

The apparent activation energy of lignin depolymerization was determined with the short column micropyrolyzer/FID, configuration described in the Materials and methods section. These tests were conducted with technical lignin to avoid polysaccharides in whole biomass contributing to the FID signal.

All samples tested with the short column micropyrolyzer/FID generated similar FID signal traces as the one illustrated in Fig. 5. Apparent activation energies for the devolatilization of lignin assuming first order reaction rates were calculated. From previous research,[8] the FID signal is known to be the result of lignin monomers released from the lignin. We speculate this is due to the breakage of lignin polymer bonds, such as the β-O-4 ether bond, and therefore devolatilization on can be used a s a proxy for the deconstruction rate. The activation energies determined from the Arrhenius plots in Fig. 6 are listed in Table 2. As a result of the high heat and mass transfer rates in the micropyrolyzer and the small size of samples, we do not think potential differences in melting of samples would affect the apparent activation energies.

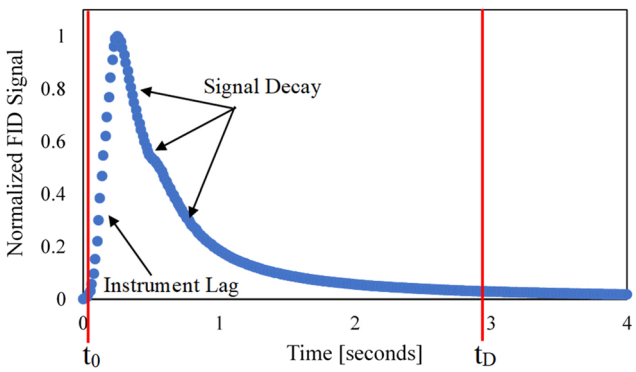

Fig. 5 FID signal response to pyrolysis of loblolly pine milled wood lignin at 400 °C. Reaction start time (t_0), 1% of maximum signal, and end time (t_D), 3% of maximum signal, are denoted by red vertical lines.

Interestingly, the apparent activation energy for lignin depolymerization in the absence of catalysts (control cases) was 40% lower for MWL from the loblolly pine *vs.* MWL from red oak. Syringyl is prominent in hardwood and lacking in softwood, this suggests that the additional methoxy group found on the aromatic ring of syringyl acts to stabilize the β-O-4 ether bond. This makes the presence of catalyst to destabilize the ether bond ever more important for hardwood lignin.

All the metals measured a decrease in apparent activation energy for lignin depolymerization. Ferrous iron proved the most powerful catalyst, reducing activation energy by 44% and 61% for red oak MWL and loblolly pine, respectively, compared to the control cases (no catalyst). These results agree with the DFT calculations, which found ferrous iron to cause the largest elongation of the C_β–O side of β-O-4 ether bonds. There was no statistical difference between the activation ener-

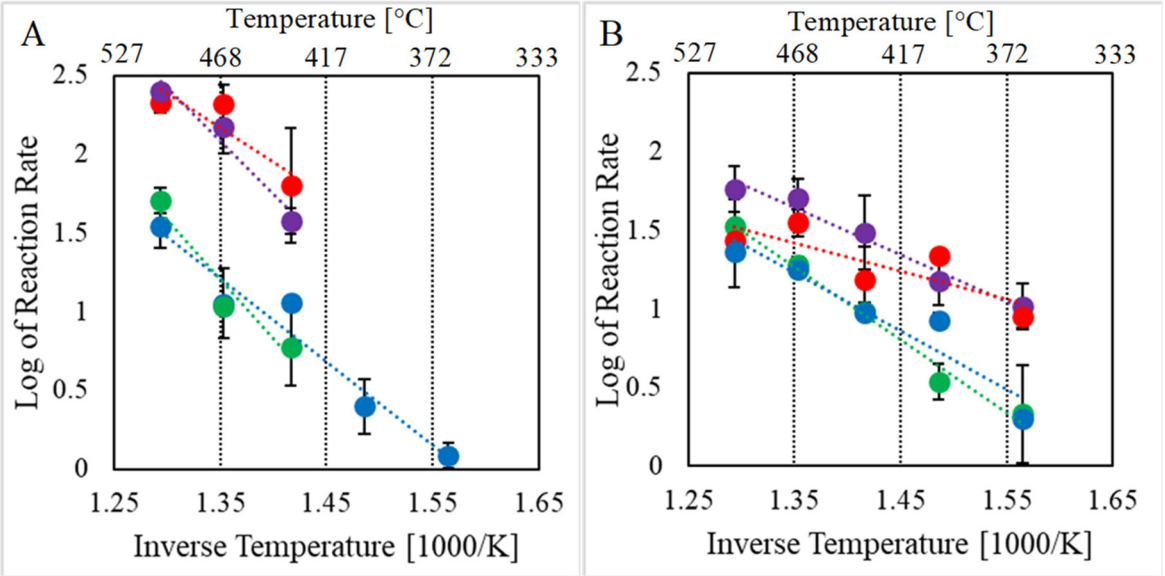

Fig. 6 Arrhenius plots for lignin fast pyrolysis devolatilization rates. (A) Red oak milled wood lignin (B) loblolly pine milled wood lignin. Data points represent triplicate tests and trend lines are linear fits. (●) Control lignin, (●) potassium acetate, (●) calcium acetate, and (●) Ferrous acetate. Error bars represent 95% confidence intervals.

Table 2 Apparent activation energies for various feedstocks from short column micropyrolysis/FID experiments. The ±represents 95% confidence intervals

Red oak milled wood lignin			Loblolly pine milled wood lignin		
Feedstock	Apparent activation energy [kcal mol^{-1}]	Apparent pre-exponential factor	Feedstock	Apparent activation energy [kcal mol^{-1}]	Apparent pre-exponential factor
Control	15.3 ± 1.9	110 000	Control	9.2 ± 0.8	1800
Ferrous iron	8.6 ± 2.3	3000	Ferrous iron	3.6 ± 0.9	49
Calcium	11.1 ± 2.8	2600	Calcium	7.5 ± 0.5	540
Potassium	13.4 ± 2.6	75 000	Potassium	6.4 ± 1.0	500

gies for calcium and potassium catalyzed depolymerization of lignin from either hardwood or softwood.

Catalyst turnover frequency (TOF) is also important in understanding lignin depolymerization. The number of bonds that must be cleaved to produce phenolic monomers from lignin is large compared to the number of metal cations available in the samples to catalyze this cleavage. Thus, if lignin is to be deconstructed in the few seconds that characterizes fast pyrolysis, these TOF must be large. The diversity of linkages in lignin prevents an exact quantitative determination of TOF. However, since the molar concentrations of catalyst was the same for all tests (1.9 mmol g^{-1}), and if the lignin is assumed to be composed of purely β-O-4 ether bonds between identical monomer units, an approximate TOF can be calculated eqn (3).

$$\mathrm{TOF} = \frac{\text{number of β-O-4 ether bonds}}{\text{number of catalyts} \times \text{reaction time}}. \quad (3)$$

We stress these values are not definitive numbers for the TOF of these catalysts but are used purely as a means of comparison between the metals in this study. As a point of reference Zhou *et al.*[24] found sodium to have a turnover frequency on cellulose of 25 s^{-1}.

Table 3 indicates that calcium has a lower TOF than either ferrous iron or potassium for both hardwood and softwood lignin. This lower TOF explains why calcium was measured to have a slower reaction rate than potassium even though their activation energies are similar. This data demonstrates the impact turnover frequency can have on a catalyst's properties. While the activation energy is important for initiating the reaction, if the catalyst is unable to migrate to other binding sites quickly its

Table 3 Approximate turnover frequency for the catalytic depolymerization of lignin at 500 °C

Red oak milled wood lignin		Loblolly pine milled wood lignin	
Catalyst	TOF [1 s^{-1}]	Catalyst	TOF [1 s^{-1}]
Ferrous iron	26	Ferrous iron	12
Calcium	12	Calcium	11
Potassium	28	Potassium	17

overall effectiveness is reduced. The practical benefit of a high turnover frequency is a reduction in the catalyst loading required for catalytic lignin deconstruction. Ferrous iron has a similar TOF as calcium and potassium in catalyzing reaction of softwood lignin. Thus, its lower activation energy makes ferrous iron an attactive catalyst for the deconstruction of softwood wood lignin. Interestingly, hardwood lignin had higher TOFs for potassium and ferrous iron catalysts but due to its higher activation energy, hardwood lignin is more difficult to deconstruct.

3.3 Investigation of internal bond changes during fast pyrolysis

The selectivity of the catalysts was assessed by investigating internal bonding changes during pyrolysis. To achieve this, experiments were conducted using the CPD-quench with the micropyrolyzer held at 500 °C to generate two samples. Truncated pyrolysis samples were ejected after reaching 400 °C, ensuring the acetate anion had decomposed and active catalyst was present, but pyrolysis was only in the initial stages. Complete pyrolysis samples were held for 60 seconds, at which point only char remained in the sample cups. By combining the truncated pyrolysis of the CPD-quench system with the structural insights provided by infrared spectroscopy the changing internal structure can be probed. Determination of lignin melting was done in a manner we previously established where in sample cups were overturned to dump out loose char then visually inspected for any residual char in the cups. The presence of residual char indicated melting had occured during pyrolysis.

The results of this testing for red oak derived MWL can be seen in Fig. 7. Both untreated and pretreated lignin have

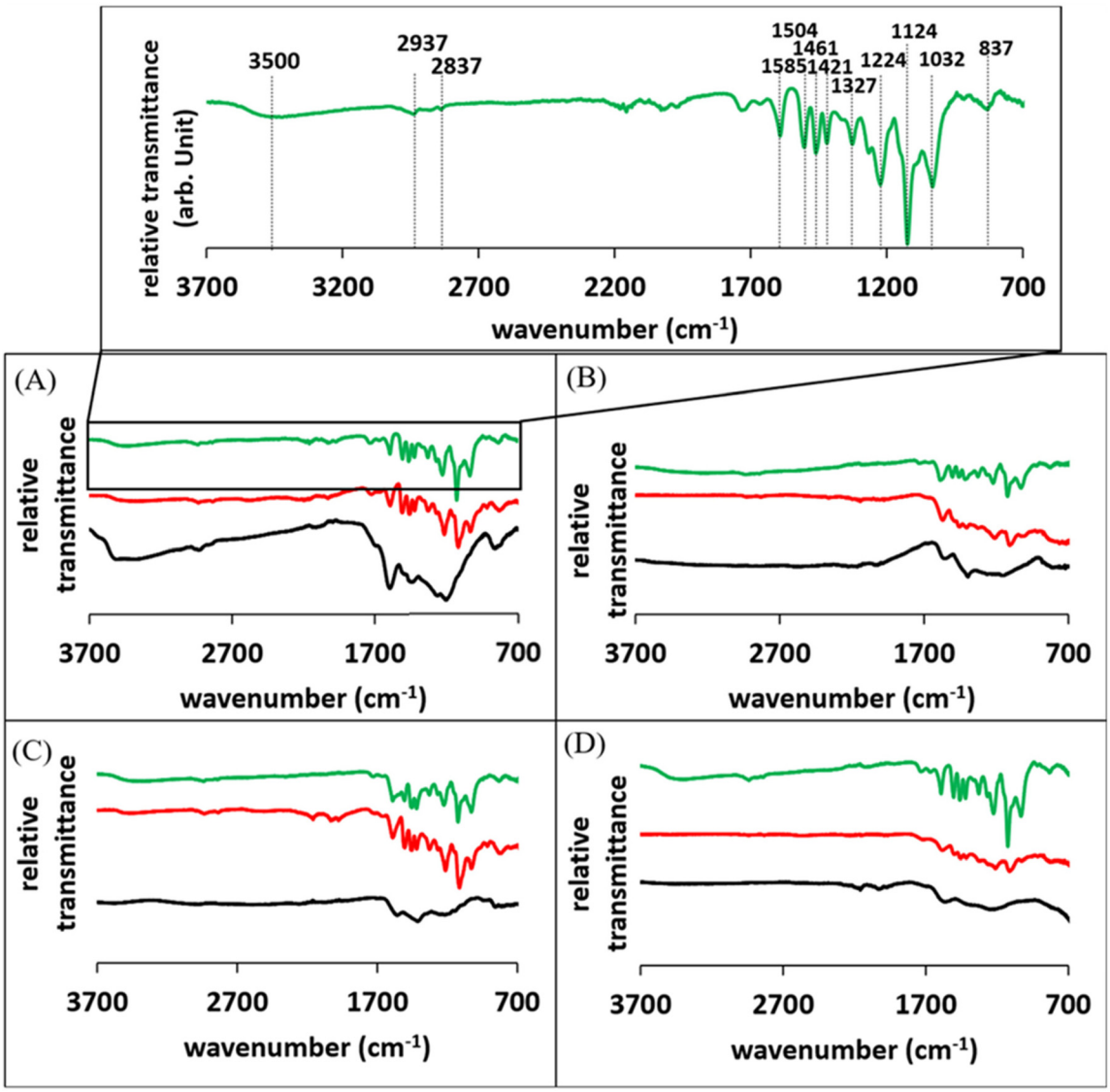

Fig. 7 FTIR spectra of red oak milled wood lignin. (A) Untreated milled wood lignin (B) potassium acetate pretreated milled wood lignin, (C) calcium acetate pretreated milled wood lignin, (D) ferrous acetate pretreated milled wood lignin. Top line represents sample before pyrolysis, middle line truncated pyrolysis after 3 seconds in a 400 °C micropyrolyzer, bottom line char remaining after 60 seconds in a 500 °C micropyrolyzer (unlabeled chart at top of figure is a magnified view of FTIR spectra for untreated milled wood lignin before pyrolysis for chart A).

several large absorption bands expected to be found in MWL. Many of these adsorption bands are attributed to the aromatic ring or side chain functional groups. The main bond of interest in this study is the β-O-4 ether linkage evident in the mirrored peaks of 1224 cm^{-1} and 1032 cm^{-1}. These twin peaks are split by the sharpest peak measured at 1124 cm^{-1} also belonging to an ether bond, in this case an aliphatic one. The lack of differences between control and pretreated lignin indicates no deconstruction has occurred during the pretreatment process.

Incomplete pyrolysis (3 s reaction duration) of untreated lignin resulted in melting but very little deconstruction. The weak ether bonds in lignin are still evident in the melted lignin indicating that melting does not involve chemical changes in the lignin. Similarly, little change is found in lignin treated with calcium during this short duration pyrolysis. In contrast, both potassium and ferrous iron pretreated lignin showed significant chemical changes as measured by FTIR spectra even though the former melted and the latter did not. The apparent activation energy for ferrous iron catalyzed lignin depolymerization was lower than for AAEM, indicating depolymerization occurs at a much lower temperature for this metal. This low activation energy explains why ferrous iron was the only catalyst that circumvented melting during the early stages of depolymerization. In contrast, while potassium has a higher TOF, its higher activation energy prevents deconstruction of lignin until the melting point of lignin is exceeded. One consequence of the lower activation energy of depolymerization is since the lignin monomers are being liberated at lower temperatures, they will also have lower vapor pressures. While product yields were not measure in this study, we suspect lower activation energies will lead to reduced product yields and result in a tradeoff between reactor operability and yield.

The char produced from complete pyrolysis of lignin showed little spectral structure under FTIR analysis. Only untreated red oak MWL had two large absorbance peaks associated with O–H bonding and aromatic oxygen, which is likely an artifact of the analysis method and not indicative of the solid char. The presence of a hydroxide group is probably a result of the severe melting that occurs with untreated lignin. Vapors formed within the melt escape as bubbles, causing the melt to foam. The melt eventually dehydrates and carbonizes, trapping gas in the voids left by the bubbles, which likely contain water and light organic compounds that are detected by FTIR when the bubbles are near the surface.

Loblolly pine MWL produced similar results as described from red oak milled wood lignin (see Fig. 8). The same absorption peaks were evident with slightly different intensities. Specifically, untreated lignin and calcium-pretreated lignin showed limited depolymerization after 3 seconds of reaction while potassium and ferrous iron pretreated lignin showed sig-

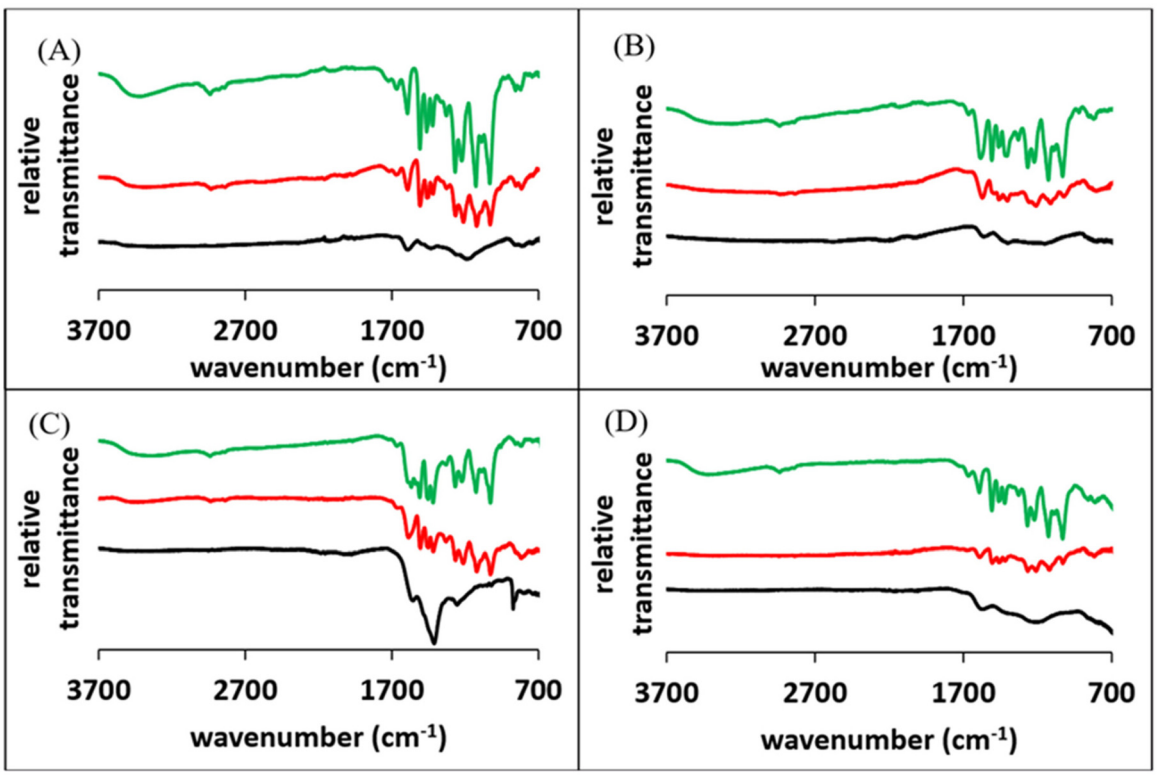

Fig. 8 FTIR spectra of loblolly pine milled wood lignin. (A) Untreated milled wood lignin, (B) potassium acetate pretreated milled wood lignin, (C) calcium acetate pretreated milled wood lignin, (D) ferrous acetate pretreated milled wood lignin. Top line represents starting biomass, middle line truncated pyrolysis 500 °C micropyrolyzer for 3 seconds, bottom line char remaining after 60 seconds in a 500 °C micropyrolyzer.

nificant depolymerization as evidenced from changes in the FTIR spectra. The strikingly large peaks observed for calcium treated char is due to the presence of a carbonate group, a decomposition product of calcium acetate. There was no large hydroxide group peak present in the untreated char as the loblolly pine lignin did not foam as severely as the red oak lignin. This was likely due to the higher deconstruction rate of softwood lignin, reducing the severity of the melt formation. Like the red oak lignin, only the ferrous iron pretreated sample of loblolly pine did not melt during pyrolysis.

4 Conclusions

This study demonstrates that ferrous iron is a much stronger lignin depolymerization catalyst compared to AAEM naturally found in biomass. However, the effectiveness of catalyst in lignin depolymerization depends upon more than simply reducing activation energy. For example, although calcium and potassium catalysts reduced apparent activation energy by a similar amount, calcium was less effective in lignin deconstruction due to a lower turnover frequency. Solving the problem of lignin melting and agglomeration during pyrolysis requires a catalyst like ferrous iron to reduce the temperature for depolymerization below the melting point for lignin. The ideal lignin depolymerization catalyst for lignin pyrolysis would combine the effectiveness of ferrous iron in bond destabilization with the high TOF of potassium. A low-cost and effective pretreatment of lignin to promote lignin depolymerization could significantly advance the pyrolysis of lignocellulosic biomass for production of fuels and chemicals.

Conflicts of interest

There are no conflicts to declare.

Acknowledgements

The authors would like to thank Malachi Hornbuckle for assistance in developing the testing procedure for short column GC experiments and Dr Santanu Bakshi for his assistance with identifying infrared absorption peaks. Kwang Ho Kim acknowledges the financial support from the Korea Institute of Science and Technology.

References

1 A. P. de Candolle, *Théorie élémentaire de la botanique; ou, Exposition des prinicpes de la classification naturelle et de l'art de décrire et d'étudier les végétaux*, Déterville, Paris, 1813.
2 H. Wang, Y. Pu, A. Ragauskas and B. Yang, *Bioresour. Technol.*, 2019, **271**, 449–461.
3 J. V. Vermaas, L. Petridis, X. Qi, R. Schulz, B. Lindner and J. C. Smith, *Biotechnol. Biofuels*, 2015, **8**, 1–16.
4 B. Shrestha, Y. Le Brech, T. Ghislain, S. Leclerc, V. Carré, F. Aubriet, S. Hoppe, P. Marchal, S. Pontvianne, N. Brosse and A. Dufour, *ACS Sustainable Chem. Eng.*, 2017, **5**, 6940–6949.
5 D. J. Nowakowski, A. V. Bridgwater, D. C. Elliott, D. Meier and P. de Wild, *J. Anal. Appl. Pyrolysis*, 2010, **88**, 53–72.
6 S. R. G. Oudenhoven, C. Lievens, R. J. M. Westerhof and S. R. A. Kersten, *Biomass Bioenergy*, 2016, **89**, 78–90.
7 V. Lago, C. Briens and F. Berruti, *Can. J. Chem. Eng.*, 2018, **96**, 132–144.
8 J. A. Tiarks, C. E. Dedic, T. R. Meyer, R. C. Brown and J. B. Michael, *J. Anal. Appl. Pyrolysis*, 2019, DOI: **10.1016/j.jaap.2019.104667**.
9 S. Ghysels, B. Dubuisson, M. Pala, L. Rohrbach, J. Van Den Bulcke, H. J. Heeres and F. Ronsse, *Green Chem.*, 2020, **22**, 6471–6488.
10 S. Zhou, R. C. Brown and X. Bai, *Green Chem.*, 2015, **17**, 4748–4759.
11 K. H. Kim, K. Jeong, S.-S. Kim and R. C. Brown, *Green Chem.*, 2019, DOI: **10.1039/c8gc02948b**.
12 K. Jeong, H. J. Jeong, G. Lee, S. H. Kim, K. H. Kim and C. G. Yoo, *Energy Fuels*, 2020, **34**, 9734–9740.
13 S. A. Rollag, J. K. Lindstrom and R. C. Brown, *Chem. Eng. J.*, 2020, **385**, 123889.
14 S. A. Rollag, J. K. Lindstrom, C. A. Peterson and R. C. Brown, *Chem. Eng. J.*, 2021, DOI: **10.1016/j.cej.2021.131882**.
15 D. J. Frisch, M. J. Trucks, G. W. Schlegel, H. B. Scuseria, G. E. Robb, M. A. Cheeseman, J. R. Scalmani, G. Barone, V. Petersson, G. A. Nakatsuji, H. Li, X. Caricato, M. Marenich, A. V. Bloino, J. Janesko, B. G. Gomperts, R. Mennucci and B. Hratch, 2016.
16 T. Lu and F. Chen, *J. Comput. Chem.*, 2012, **33**, 580–592.
17 F. Weinhold and C. R. Landis, *Chem. Educ. Res. Pract.*, 2001, **2**, 91–104.
18 A. Björkman, *Sven. Papperstidn.*, 1956, **59**, 477–485.
19 H. Liu, J. Y. Zhu and S. Y. Fu, *J. Agric. Food Chem.*, 2010, **58**, 7233–7238.
20 C. A. Peterson, M. K. Hornbuckle and R. C. Brown, *Fuel Process. Technol.*, 2022, **226**, 107068.
21 J. K. Lindstrom, J. Proano-Aviles, P. A. Johnston, C. A. Peterson, J. S. Stansell and R. C. Brown, *Green Chem.*, 2019, **21**, 178–186.
22 J. Proano-Aviles, J. K. Lindstrom, P. A. Johnston and R. C. Brown, *Energy Technol.*, 2017, **5**, 189–195.
23 P. Virtanen, R. Gommers, T. E. Oliphant, M. Haberland, T. Reddy, D. Cournapeau, E. Burovski, P. Peterson, W. Weckesser, J. Bright, S. J. van der Walt, M. Brett, J. Wilson, K. J. Millman, N. Mayorov, A. R. J. Nelson, E. Jones, R. Kern, E. Larson, C. J. Carey, İ. Polat, Y. Feng, E. W. Moore, J. VanderPlas, D. Laxalde, J. Perktold, R. Cimrman, I. Henriksen, E. A. Quintero, C. R. Harris, A. M. Archibald, A. H. Ribeiro, F. Pedregosa, P. van Mulbregt, A. Vijaykumar, A. Pietro Bardelli, A. Rothberg, A. Hilboll, A. Kloeckner, A. Scopatz, A. Lee, A. Rokem, C. N. Woods, C. Fulton,

C. Masson, C. Häggström, C. Fitzgerald, D. A. Nicholson, D. R. Hagen, D. V. Pasechnik, E. Olivetti, E. Martin, E. Wieser, F. Silva, F. Lenders, F. Wilhelm, G. Young, G. A. Price, G. L. Ingold, G. E. Allen, G. R. Lee, H. Audren, I. Probst, J. P. Dietrich, J. Silterra, J. T. Webber, J. Slavič, J. Nothman, J. Buchner, J. Kulick, J. L. Schönberger, J. V. de Miranda Cardoso, J. Reimer, J. Harrington, J. L. C. Rodríguez, J. Nunez-Iglesias, J. Kuczynski, K. Tritz, M. Thoma, M. Newville, M. Kümmerer, M. Bolingbroke, M. Tartre, M. Pak, N. J. Smith, N. Nowaczyk, N. Shebanov, O. Pavlyk, P. A. Brodtkorb, P. Lee, R. T. McGibbon, R. Feldbauer, S. Lewis, S. Tygier, S. Sievert, S. Vigna, S. Peterson, S. More, T. Pudlik, T. Oshima, T. J. Pingel, T. P. Robitaille, T. Spura, T. R. Jones, T. Cera, T. Leslie, T. Zito, T. Krauss, U. Upadhyay, Y. O. Halchenko and Y. Vázquez-Baeza, *Nat. Methods*, 2020, **17**, 261–272.

24 X. Zhou, H. B. Mayes, L. J. Broadbelt, M. W. Nolte and B. H. Shanks, *AIChE J.*, 2016, **62**, 766–777.